

High-resolution statistical mapping reveals gene territories in live yeast

Axel B Berger¹, Ghislain G Cabal^{1,7}, Emmanuelle Fabre², Tarn Duong³, Henri Buc⁴, Ulf Nehrass^{1,7}, Jean-Christophe Olivo-Marin⁵, Olivier Gadal^{1,6} & Christophe Zimmer³

The nonrandom positioning of genes inside eukaryotic cell nuclei is implicated in central nuclear functions. However, the spatial organization of the genome remains largely uncharted, owing to limited resolution of optical microscopy, paucity of nuclear landmarks and moderate cell sampling. We developed a computational imaging approach that creates high-resolution probabilistic maps of subnuclear domains occupied by individual loci in budding yeast through automated analysis of thousands of living cells. After validation, we applied the technique to genes involved in galactose metabolism and ribosome biogenesis. We found that genomic loci are confined to 'gene territories' much smaller than the nucleus, which can be remodeled during transcriptional activation, and that the nucleolus is an important landmark for gene positioning. The technique can be used to visualize and quantify territory positions relative to each other and to nuclear landmarks, and should advance studies of nuclear architecture and function.

The spatial organization of the genome inside eukaryotic cell nuclei is not random, and has a central role in transcriptional regulation, DNA repair and replication¹. Despite many studies, this organization remains poorly understood. Chromosomes 'painted' by fluorescence *in situ* hybridization in fixed vertebrate cells occupy distinct volumes, termed chromosome territories², but individual genetic loci can be detected in and out of such territories³. Recent analyses of subnuclear locus positions using precise optical measurements had been similarly restricted to fixed cells^{4,5}. In the budding yeast *Saccharomyces cerevisiae*, in which the existence of chromosome territories is disputed^{6,7}, but in which expression studies and endogenous fluorescent tagging are relatively straightforward⁸, several microscopy studies could link subnuclear gene location to gene activity^{9–14}.

Current imaging studies of nuclear organization suffer from important limitations. First, locus positions are generally described

only by distance to the nuclear envelope or center, thus reducing compartmentalization to averages in spherical shells and one-dimensional (1D) radial distance histograms, even when images are three-dimensional (3D)¹⁵. These 1D descriptions do not account for the geometry of interphase yeast nuclei, where chromosome centromeres are anchored via microtubules and kinetochores to the spindle pole body (SPB), a protein structure embedded in the nuclear envelope¹⁶. This attachment results in a chromosome configuration that violates spherical symmetry^{17,18}. Radial analyses also ignore the nucleolus and thus its role in positioning tRNA genes¹⁹ or ribosomal protein genes²⁰. Second, optical microscopy studies have a diffraction-limited resolution of at best ~250–500 nm, thus strongly blurring subcompartments inside yeast nuclei (~1 μm radius). Third, for lack of automation, at most a few hundred or tens of nuclei have been analyzed in static or dynamic imaging studies, respectively. However, because of stochastic motions, gene compartmentalization is at best probabilistic and must be assessed statistically from large populations.

On account of these limitations, spatial nuclear organization and hence its regulatory potential are probably strongly underestimated. Here we describe a computational imaging technique that overcomes these obstacles and generates high resolution probabilistic two-dimensional (2D) maps of gene localization from thousands of cells, which allows for accurate dissection of yeast nuclear architecture *in vivo*. Using this technique, we observed spatial segregation of coregulated galactose genes, nucleolar localization of several ribosome biogenesis genes and strong gene compartmentalization within the small yeast nucleus.

RESULTS

Automated localization of genes and nuclear landmarks

To analyze the spatial location of a given locus in a coordinate frame intrinsic to the *S. cerevisiae* nucleus, we determined the 3D position of the locus relative to the nuclear envelope, the nuclear center and

¹Institut Pasteur, Unité de Biologie Cellulaire du Noyau, Centre National de la Recherche Scientifique, Unité de Recherche Associée 2582, ²Institut Pasteur, Unité de Génétique Moléculaire des Levures, Centre National de la Recherche Scientifique, Unité de Recherche Associée 2171, ³Institut Pasteur, Groupe Imagerie et Modélisation, Centre National de la Recherche Scientifique, Unité de Recherche Associée 2582, ⁴Institut Pasteur, Département de Biologie Cellulaire et Infections, and ⁵Institut Pasteur, Unité d'Analyse d'Images Quantitative, Centre National de la Recherche Scientifique, Unité de Recherche Associée 2582, 25-28 rue du Docteur Roux, 75015 Paris, France. ⁶Laboratoire de Biologie Moléculaire des Eucaryotes, Centre National de la Recherche Scientifique, Unité Mixte de Recherche 5099, Université de Toulouse, 118 route de Narbonne, 31000 Toulouse, France. ⁷Present addresses: Instituto de Medicina Molecular, Unidade de Malaria, Av. Professor Egas Moniz, 1649-028 Lisboa, Portugal (G.G.C.) and Institut Pasteur Korea, 39-1, Hawolgok-dong, Sungbuk-gu, Seoul 136-791, Korea (U.N.). Correspondence should be addressed to C.Z. (czimmer@pasteur.fr) or O.G. (olivier.gadal@ibcg.biotoul.fr).

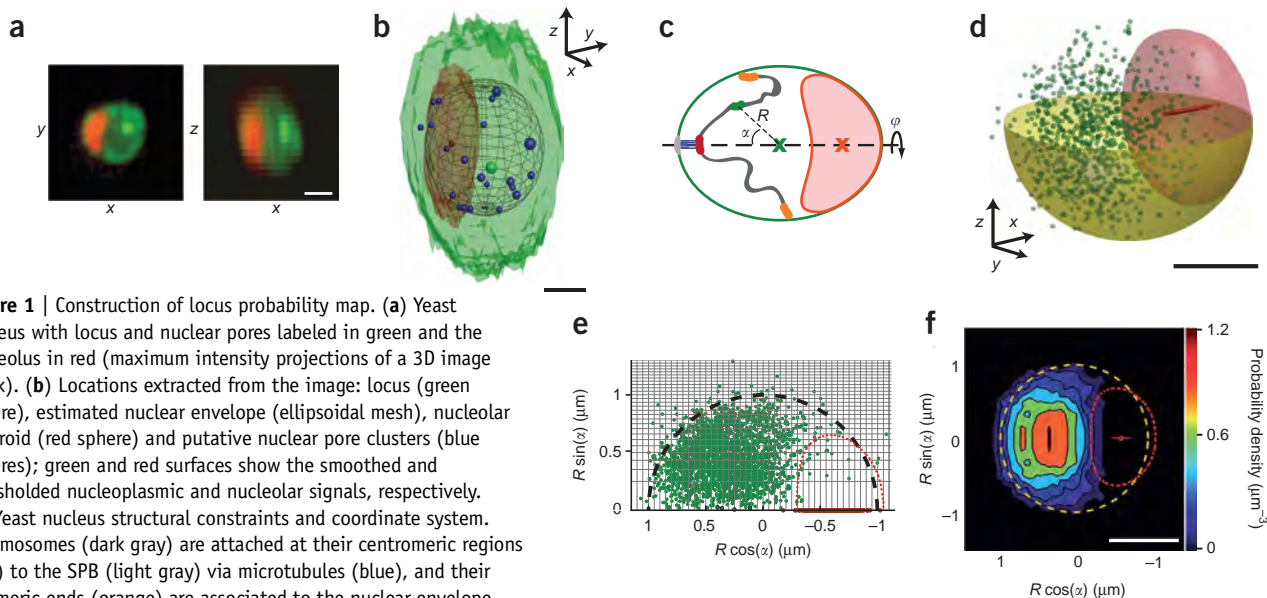


Figure 1 | Construction of locus probability map. **(a)** Yeast nucleus with locus and nuclear pores labeled in green and the nucleolus in red (maximum intensity projections of a 3D image stack). **(b)** Locations extracted from the image: locus (green sphere), estimated nuclear envelope (ellipsoidal mesh), nucleolar centroid (red sphere) and putative nuclear pore clusters (blue spheres); green and red surfaces show the smoothed and thresholded nucleoplasmic and nucleolar signals, respectively. **(c)** Yeast nucleus structural constraints and coordinate system. Chromosomes (dark gray) are attached at their centromeric regions (red) to the SPB (light gray) via microtubules (blue), and their telomeric ends (orange) are associated to the nuclear envelope (green oval). The ‘central axis’ (dashed line) joins the nuclear center (green X) and the centroid (red X) of the nucleolus (shaded, red). R , radial distance of locus to nuclear center; α , elevation angle from central axis; and φ , azimuthal angle around central axis. **(d)** A 3D view of *URA3* locus positions (green spheres) obtained from 2,485 nuclei, after nuclear landmark alignment; red spheres indicate nucleolar centroids; yellow hemisphere radius, 1 μm ; the red surface shows the ‘median’ nucleolus. **(e)** Locus positions in cylindrical coordinates with 1 μm -radius half-circle, projected nucleolar outline and histogram grid. **(f)** *URA3* probability density map based on analysis of 2,485 nuclei grown in glucose-containing medium. Top and bottom halves are mirrored for visual convenience only. Dashed circle, ‘median’ nuclear envelope; dashed red curve, ‘median’ nucleolus; small red circle, median location of nucleolar centroid; red bar, range between the percentiles 10 and 90 of the nucleolus centroid position. Scale bars, 1 μm .

the nucleolus, as landmarks. To fluorescently tag single loci, we inserted *TetO* repeats, which were targeted by the fusion protein TetR-GFP. We additionally expressed the nuclear pore protein Nup49, also fused to GFP¹¹, to visualize the nuclear envelope and the red fluorescent protein mCherry²¹ fused to the nucleolar protein Nop1 to identify the nucleolus. We imaged asynchronous live-cell populations in three dimensions, yielding images containing up to ~ 200 cells each (Supplementary Notes 1 and 2 online).

We developed computational tools to extract accurate positional information from thousands of cells (Supplementary Note 3 online). Briefly, an automated module detected individual interphase cells (G1 and S phase) in the fluorescence image; alternatively, a user could manually select cells of a particular phase by inspecting their morphology in combined fluorescence and transmission microscopy images (Supplementary Fig. 1 online). Next, for each individual cell, we computed the 3D coordinates of the fluorescent locus, nuclear center and nucleolar ‘centroid’, estimated an ellipsoid approximating the nuclear envelope and segmented the nucleolus (Fig. 1a,b). All extracted localizations were corrected for chromatic shifts and finally subjected to an automatic quality control to limit processing errors. We estimated the accuracy of measured locus positions relative to nuclear center and nucleolar centroid (σ_l) to be ~ 30 nm (Supplementary Note 4 online). Thus, the method extracted 3D positions of loci and nuclear landmarks with high accuracy in thousands of living yeast cells.

Construction of high-resolution probabilistic gene maps

The extracted localizations allowed us to compute distances of loci to the nuclear envelope, the nuclear center or nucleolar centroid. They also enabled us to define a cylindrical coordinate system adapted to the yeast nuclear geometry¹⁸ with an oriented ‘central

axis’ passing through the nuclear center and nucleolar centroid (Fig. 1c). Because this axis crosses the nuclear envelope near the SPB^{22,23}, the genetic material should be organized around it. Therefore, we described the position of a locus by its distance from the nuclear center (R) and angle from the central axis (α) (Fig. 1c).

Although distributions of R or α in cell populations can be analyzed separately as 1D histograms or cumulative frequency plots (Supplementary Fig. 2 online), more information is gained from joint distributions (R , α). Because 2D distributions require considerably more cells than 1D histograms to ensure robust statistics, we analyzed $\sim 1,000$ – $5,000$ cells in each population (Table 1). We then aggregated the extracted positions into a single probabilistic map. To do this, we aligned the nuclear landmarks of different nuclei by translations to move nuclear centers to the origin, followed by rotations around the origin that moved nucleolar centroids onto the half-axis, $\alpha = 180^\circ$ (the line originating from the nuclear center and going through the nucleolar centroid) (Fig. 1d). The absence of a third nuclear landmark left the angle around the central axis (φ) undefined. To facilitate visualization, we took advantage of this degree of freedom and rotated all loci around the central axis and into a single plane essentially without loss of information (Fig. 1e).

From this 2D distribution of points, we then estimated the underlying probability density, that is, the probability per unit volume (Supplementary Note 5 online). Briefly, we computed the isocontours of a ‘blurred’ 2D histogram. We chose the histogram grid such that volumes projected in each bin were equal, thereby ensuring uniform statistical weights (Fig. 1e). To visualize the typical nuclear size, we overlaid a circle with a radius equal to the population median of $(R_x + R_y + R_z)/3$, where R_x , R_y , R_z are the semi-axes of the nuclear envelope ellipsoid. Likewise, we plotted a ‘median’ nucleolar outline representing the typical shape of the nucleolus.

Table 1 | Sizing gene territories

Locus	Territory size		V_{Nu} (μm^3)	R_N (μm)	V_{No} (μm^3)	n	P_{max} (μm^{-3})	$1/V_{Nu}$ (μm^{-3})	G1/S	d_{CEN} (kb)
	(μm^3)	(% V_{Nu})								
rDNA	0.53	13.9	4.46	0.97	1.24	2,663	1.14	0.26	2.3	300–2,300
CEN	0.97	15.3	6.11	1.15	1.38	657	0.93	0.16	1.7	NA
Tel VIII	1.45	31.4	3.8	1.03	1.25	1,395	0.44	0.22	1.8	482
<i>GAL1</i> , glucose	0.58	16.5	3.5	0.95	1.14	1,857	1.65	0.29	1.7	42
<i>GAL1</i> , galactose	0.9	26.2	3.39	0.94	0.62	1,702	0.60	0.30	1.8	42
<i>GAL2</i> , glucose	0.86	23.5	3.62	0.96	1.08	2,083	1.11	0.28	–	139
<i>GAL2</i> , galactose	0.51	16.3	3.07	0.91	0.61	1,703	1.31	0.33	–	139
<i>gal2Δ</i> , glucose	0.74	18.6	3.9	0.98	1.03	1,981	1.13	0.26	–	139
<i>gal2Δ</i> , galactose	0.59	16.1	3.62	0.96	0.50	1,704	0.90	0.28	–	139
<i>URA3</i> , glucose	0.64	18.4	3.5	0.94	1.1	2,485	1.23	0.29	1.6	35
<i>URA3</i> , galactose	0.63	19.9	3.1	0.91	0.65	2,375	1.29	0.32	2.1	35
<i>HMO1</i>	1.32	28.8	4.55	1.04	0.96	3,823	0.80	0.22	1.6	362
<i>SNR17A–RPL33B</i>	1.48	26.9	5.5	1.10	1.27	3,521	0.64	0.18	1.6	451
<i>RPS5</i>	1.7	33.2	4.47	1.03	1.20	4,289	0.36	0.24	1.6	215
<i>RPS20</i>	0.8	17.4	4.46	1.03	1.19	3,543	1.12	0.22	1.9	30
Random nucleus	1.8	43.3 ± 0.6	4.19	1.00	0	2,000	0.3	0.24	NA	NA
Random nucleoplasm	1.6	38.1 ± 0.7	4.19	1.00	1.24	2,000	0.4	0.24	NA	NA

Territory sizes, in cubic micrometers and as percentage of the median estimated nuclear volume V_{Nu} (% V_{Nu}). n , number of cells analyzed. V_{No} , median estimated nucleolar volume. R_N , median nuclear envelope radius. d_{CEN} , genomic distance to centromere. G1/S, ratio of cells in G1 and S phase, averaged from two independent counting experiments on ~200–500 cells for each population, except for *GAL2*. Values for random distributions were computed from 10 simulations of 2,000 points each with constant probability density inside a sphere (nucleus) or a capped sphere (nucleoplasm) and with added random positioning errors of s.d. 30 nm; cap volume was 20% of the sphere, the average estimated fraction of V_{Nu} occupied by the nucleolus. $1/V_{Nu}$ is the average expected probability density for a random nuclear distribution. Note that territory volumes are estimated assuming that probability densities are cylindrically symmetric around the central axis and constant within each histogram bin; hence, they likely overestimate the true 3D volumes. –, not measured; NA, not applicable.

As a first example, we considered gene *URA3*. Its probability map showed that *URA3* can occupy any subnuclear location except the nucleolus but was preferentially located in a region roughly half-way between the nuclear center and the nuclear envelope and close to the central axis (Fig. 1f). To quantify this probabilistic confinement, we defined the ‘gene territory’ as the region covered by the smallest set of histogram bins containing 50% of observed locus positions (Supplementary Fig. 3 online). Note that this notion is distinct from that of chromosome territories, which can be identified by chromosome painting in single cells². We then computed the gene territory volume. *URA3* occupied a territory of $0.64 \mu\text{m}^3$, ~0.18 of the median nuclear volume, V_{Nu} . The latter value can be compared to that expected from a uniformly random distribution inside the entire nucleus or nucleoplasm (nuclear volume excluding the nucleolus), for example, 0.43 of V_{Nu} and 0.38 of V_{Nu} , respectively, for 2,000 cells (Table 1). Thus, *URA3* was concentrated within less than half of the nuclear or nucleoplasmic volume. Alternatively, the maximum probability density (P_{max}) can be compared to the average probability density expected for random distributions, with higher ratios indicating stronger confinement; for *URA3*, this ratio was roughly 4 (Table 1).

Unlike for the original microscopy images, the resolution of the probability maps is not limited by diffraction but by random errors in the position measurements of single loci. The estimated positioning accuracy, σ_l , of ~30 nm translates into a theoretical map resolution of < ~100 nm, but in practice resolution is also limited by the coarseness of the histogram grid, and hence depends both on direction and subnuclear location (Supplementary Note 6 online). With the grid we chose here, the estimated resolution was better than 150 nm in approximately 80% of the volume of a spherical 1 μm radius nucleus.

Therefore, our technique can map and quantify the probabilistic subnuclear space occupied by genomic loci in living cells at estimated subdiffraction resolution with a commercial microscope and standard fluorescence labeling.

Probability maps recover yeast nuclear architecture

To validate the method’s ability to characterize nuclear architecture, we first mapped the SPB. If the technique is accurate, the probability map should peak where the nuclear envelope intersects the central axis ($\alpha = 0$). Identifying the SPB by labeling its central protein component, Spc29, we observed a signal similar in intensity to a labeled locus. The SPB probability indeed strongly peaked at the expected location (Fig. 2a). The median ‘signed’ distance (d) of the SPB tag to the nuclear envelope was only 13 nm (Supplementary Fig. 2a), implying that the median nuclear envelope was located very accurately (nuclear envelope estimation for individual cells was less accurate, as the s.d. of d was 141 nm). Second, we examined a single unit of ribosomal DNA, known to cluster near or within the nucleolus²³. Its probability map featured a small ($0.53 \mu\text{m}^3$ or 0.14 of V_{Nu} ; Table 1) crescent-shaped territory typical of the nucleolus and was in excellent agreement with the median nucleolar outline (Fig. 2b). Third, we analyzed a centromeric plasmid, which occupied a ~1 μm^3 territory (0.15 of V_{Nu}) near the central axis and the SPB, at ~300–700 nm from the median nuclear envelope (Fig. 2c). This agrees with distances measured previously between SPB and a chromosomal centromere visualized simultaneously²⁴. Finally, we mapped a subtelomeric locus and found it excluded from the nucleolar region and concentrated in a $1.45 \mu\text{m}^3$ territory (0.31 of V_{Nu}) near the nuclear envelope, again as expected^{17,18} (Fig. 2d). For comparison, we also mapped a simulated random nuclear localization (Fig. 2e).

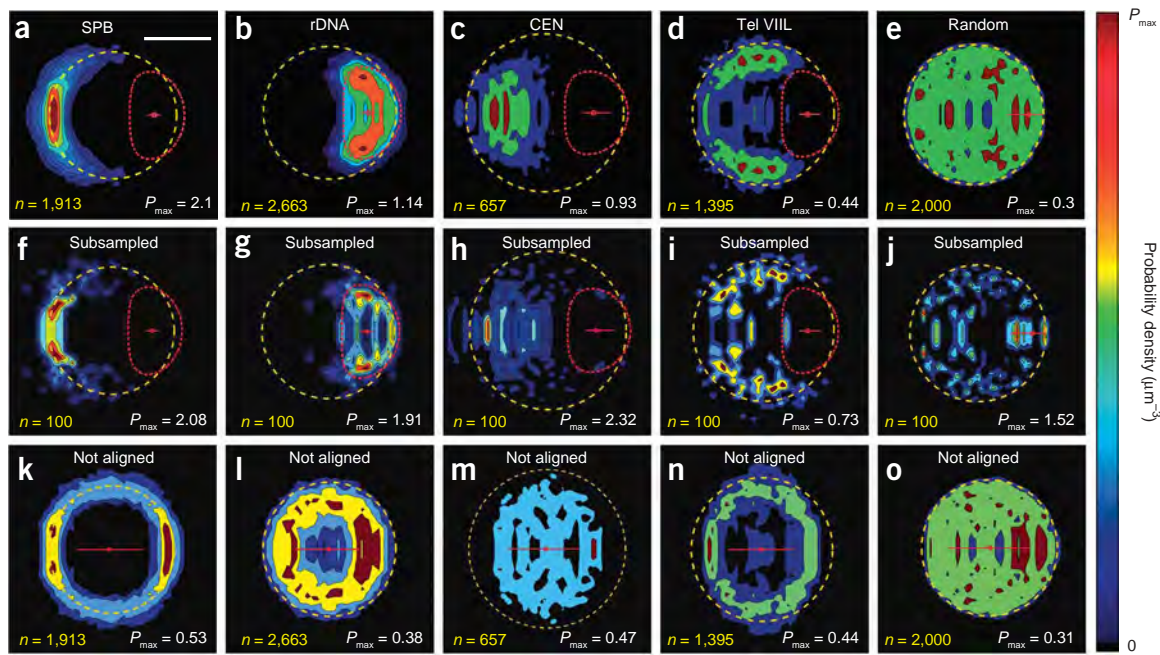


Figure 2 | Validation of mapping method for different loci and the SPB. (a–o) Probability maps as in **Figure 1f** (a–d, simulated map in e), maps obtained using only 100 cells (f–j) and maps obtained without alignment of the nucleolar centroid (k–o), of the SPB protein Spc29 (a,f,k), rDNA locus (b,g,l), centromeric plasmid (c,h,m), subtelomere on the left arm of chromosome 7 (d,i,n) and a simulated point randomly located within the nuclear volume (e,j,o). The color bar indicates probability density from 0 to P_{\max} . Scale bar, 1 μm .

Therefore, our approach provided quantitative measurements and visualizations of subnuclear territories that agree with established notions of nuclear organization. The maps were considerably less accurate and noisier when cell number was reduced to 100 (**Fig. 2f–j**). Similarly, compartmentalization was lost in the absence of nucleolar alignment (**Fig. 2k–o**). This underscores the importance of large samples and nuclear landmark alignment, two key features of our method.

Remodeling of gene territories upon activation

To demonstrate the method's potential for functional studies of nuclear organization, we revisited the repositioning of galactose genes upon transcriptional activation^{10–12} (**Fig. 3**). We first analyzed the gene cluster *GAL7-GAL10-GAL1* (hereafter referred to as *GAL1*) and found that in presence of glucose, where the gene is repressed, *GAL1* concentrates in a small $0.58 \mu\text{m}^3$ territory close to the nuclear center (**Fig. 3a**), whereas in presence of galactose, where *GAL1* is active, its territory expands to $0.9 \mu\text{m}^3$ and is enriched near the nuclear periphery (1D χ^2 -test on signed distances: $P_1 < 10^{-4}$; 2D χ^2 -test on point distributions: $P_2 < 10^{-4}$; **Supplementary Fig. 2a,b** and **Supplementary Note 7** online), confirming published results^{11,12}. Notably, the territory clearly split into two regions: one close to the nuclear center, as in the repressed state, another one close to the SPB (**Fig. 3b**). Combined with the earlier observation that *GAL1* mRNA is detected when the locus is preferentially peripheral¹¹, this result supports a model where the on/off states of transcription correspond to two location states. Note that the bimodality disappeared in the absence of nucleolar alignment (**Fig. 3c,d**) and was therefore not apparent from previous static analyses. This result lends strong statistical support to earlier dynamic data suggesting two spatial states for *GAL1* (ref. 11).

An alternative possibility is that the switch in growth medium altered the cell cycle, which in turn might affect locus positioning²⁵. However the proportion of cells exhibiting peripheral versus central *GAL1* was similar in G1 and S phase (data not shown). The nucleolar volume in the presence of galactose was roughly halved compared to that in glucose, while nuclear volumes were reduced only slightly (**Table 1**). To examine whether relocalization resulted from medium-dependent alterations of nucleolar morphology, we mapped *URA3*, whose expression is not affected by the switch from glucose to galactose, and which occupied a territory similar to *GAL1* in glucose (**Figs. 1f** and **3a**). No significant change in *URA3* localization was visible in galactose ($P_1 = 0.12$; $P_2 = 0.26$), confirming the activation-dependent nature of *GAL1* territory remodeling (**Supplementary Fig. 4a,b** online).

We next examined *GAL2*, which is activated by the same upstream activated sequences and binding factors as *GAL1*¹⁰. Like *GAL1*, *GAL2* is known to relocalize toward the periphery upon activation¹⁰, suggesting that both genes are recruited to nuclear pores where they possibly share the same transcription machinery^{3,26}. Probability maps showed that *GAL2* was confined to a small ($0.86 \mu\text{m}^3$) territory between the nucleolus and the nuclear center when repressed (**Fig. 3e**). Upon galactose induction, the *GAL2* territory slightly shifted toward the nuclear periphery ($P_1 < 10^{-4}$), consistent with earlier findings¹⁰ (**Fig. 3f,m**). However, whereas activated *GAL1* partly concentrated near the nuclear periphery and the SPB, activated *GAL2* accumulated near the nucleolus. Thus, *GAL2* was juxtaposed less frequently with the nuclear envelope than *GAL1* but more often with the nucleolus. Furthermore, activated *GAL1* and *GAL2* occupied largely distinct territories and are thus unlikely to be transcribed by the same transcription machinery (**Fig. 3b,f**).

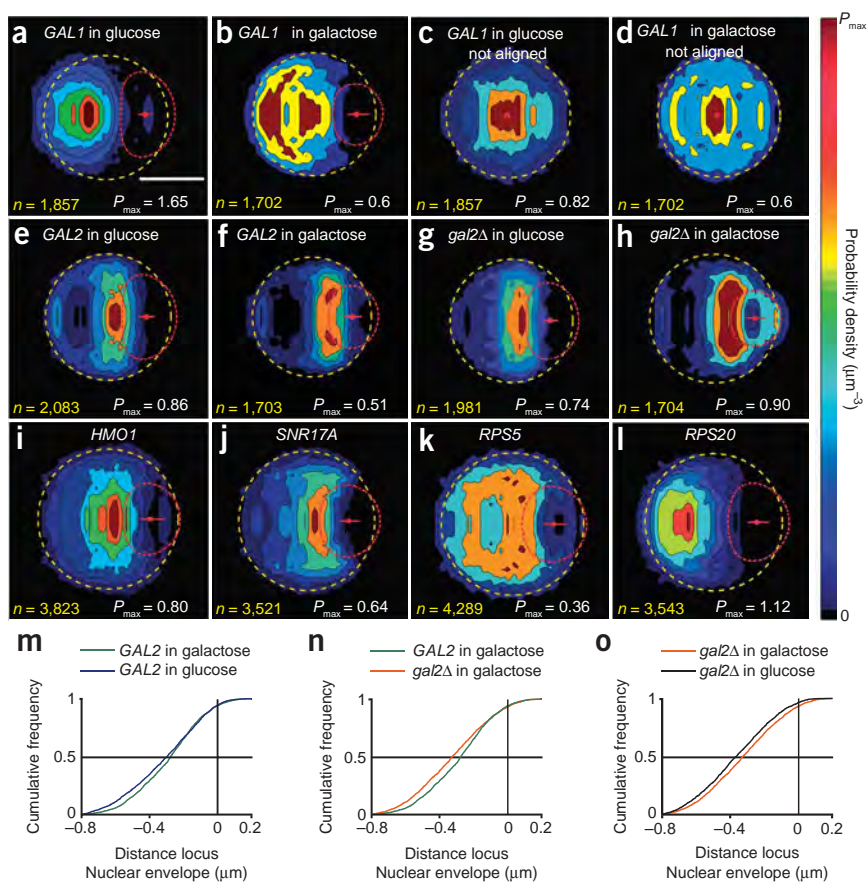


Figure 3 | Probability maps of genes involved in galactose metabolism and ribosome biogenesis. (a,b) Map of *GAL1* in medium containing glucose (a) and galactose (b). (c,d) Same as a and b, but without alignment of nucleolar centroids. (e,f) Map of *GAL2* in medium containing glucose (e) and galactose (f). (g,h) Map of *GAL2* locus in *gal2Δ* mutant cells in medium containing glucose (g) and galactose (h). (i–l) Maps of *HMO1* (i), *SNR17A–RPL33B* (j), *RPS5* (k) and *RPS20* (l) loci. (m–o) Distance of *GAL2* locus to nuclear envelope (cumulative frequencies): *GAL2* in galactose versus *GAL2* in glucose (m), *GAL2* in galactose versus *gal2Δ* in galactose (n) and *gal2Δ* in glucose versus *gal2Δ* in galactose (o). Scale bar, 1 μm.

precursor rRNA gene and the polymerase III (Pol III)-transcribed 5S rRNA gene, both located at the same site on chromosome 12, and for Pol III-transcribed tRNA coding genes, scattered across all chromosomes¹⁹. We first mapped gene *HMO1* located on chromosome 4. The protein Hmo1 is involved in transcription of both rDNA and of genes encoding ribosomal proteins, thus providing a link between Pol I- and Pol II-mediated transcription²⁷. *HMO1* occupied a central territory close to the nucleolus, much like *GAL2*, albeit ~1.5–2 times larger (Fig. 3i and Table 1). The noncoding snoRNA U3 is required for the first processing step of ribosomal RNA and is coded by *SNR17A* and *SNR17B*, on chromosomes 15 and 16, respectively. Mapping indicated that *SNR17A* again occupied a perinucleolar territory, similar to *HMO1* (Fig. 3j). Because *SNR17A* is only 0.7 kilobases (kb) away from gene *RPL33B*, these data implied that both a noncoding snoRNA gene and a ribosomal protein gene were associated with the nucleolus.

To test whether this association holds for other ribosomal protein genes, we investigated *RPS5* and *RPS20*, on chromosomes 10 and 8, respectively. *RPS5* was also enriched near the nucleolus (1D χ^2 -test

Unlike *GAL1*, *GAL2* was juxtaposed to the nucleolus in both growth media and lies on the same arm of chromosome 12 as the rDNA. Therefore, the observed slight peripheral shift of this locus upon switch to galactose-containing medium possibly resulted from the reduced nucleolar size in galactose, rather than from gene activation. Analyzing the deletion mutant *gal2Δ*, we found the *GAL2* site to be slightly less peripheral than in wild-type cells, both in glucose and galactose, as previously reported¹⁰ ($P_1 < 10^{-4}$) (Fig. 3g,h,n). However, we still observed a moderately significant increase in peripheral occupancy upon shift to galactose in *gal2Δ* ($P_1 = 0.035$) (Fig. 3o). Therefore, although consistent with the observation that *GAL2* regulatory sequences are required for increased peripheral occupancy in wild-type cells¹⁰, our results suggest that *GAL2* relocalization is caused at least partly by medium-dependent nucleolar reorganization. To address possible influences of cell-cycle alterations caused by the mutant or growth medium, we mapped *GAL2* in G1 cells only and found no noticeable difference in localization (Supplementary Fig. 4c–f), again ruling out substantial cell-cycle effects.

Thus, the mapping technique could show that two co-regulated *GAL* genes occupy different subnuclear territories, and suggests that the nucleolus is an important structural element for positioning of genes on chromosome 12.

Nucleolar association of ribosome biogenesis genes

We next investigated polymerase II (Pol II)-transcribed genes required for ribosomal biogenesis and located on other chromosomes. Spatial association with the nucleolus was previously documented only for the polymerase I (Pol I)-transcribed 35S

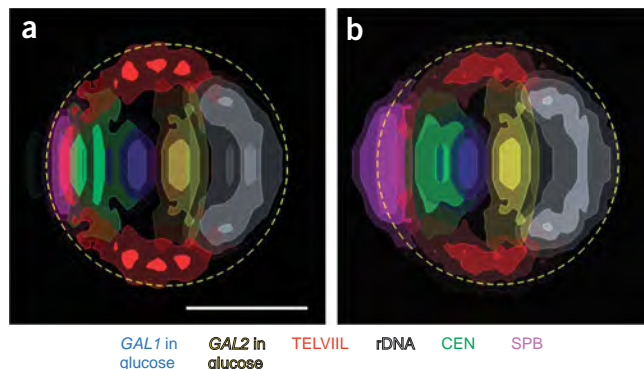


Figure 4 | Visualizing the spatial arrangement of gene territories. (a,b) Combined maps showing relative arrangement of five selected gene territories and the SPB, as indicated by the color labels. In a, individual probability maps from Figures 2 and 3 were superposed without transformation. Locus coordinates x , y and z were linearly scaled to the nuclear envelope ellipsoid semi-axes (R_x , R_y , R_z) before maps were superposed in b. Note how different loci occupy largely distinct subnuclear territories. Scale bar, 1 μm.

on $R \cos(\alpha)$ compared to a constant distribution: $P'_1 < 10^{-4}$; **Supplementary Note 7**), though more dispersed than *HMO1* and *SNR17A* (**Fig. 3k**). In contrast, *RPS20* was distant from both the nucleolus and the nuclear envelope, and close to the centromeric territory (**Fig. 3l**).

Spatial arrangement of gene territories

Because the number of spectrally distinguishable dyes available for live-cell labeling is limited, it is difficult to simultaneously localize many genes inside the same cell. Nevertheless, one can visualize the spatial arrangement of gene territories by superposing color-coded maps of different loci. We first did this without rescaling, thus preserving spatial distances (**Fig. 4a**). As nuclear sizes vary between cell populations (**Table 1**), the actual territory arrangement within a population may differ. Therefore, we next linearly scaled 3D coordinates to warp the nuclear envelope into a unit sphere (**Fig. 4b**). For the loci examined here, this scaling slightly changed territory locations, but left relative positioning unaffected (**Fig. 4**). Both maps showed a remarkably high degree of spatial organization, with several territories appearing juxtaposed to each other with relatively limited overlap.

What determines gene territory location? From the geometrical constraints on chromosomes sketched in **Figure 1c**, loci at small genomic distance to the centromeric region (d_{CEN}) are expected to occupy territories spatially closer to the SPB or the centromere territory, whereas loci at larger d_{CEN} should be closer to the nucleolus. To verify this quantitatively, we plotted the median abscissa along the central axis against d_{CEN} . The plot qualitatively confirmed the expected trend, but also displayed a surprisingly consistent linear dependence at genomic and spatial scale ranges ~ 50 – 500 kb and ~ 0.05 – 0.5 μm , respectively (exceptions are the nuclear envelope-associated telomere and *GAL2*, which lies on the rDNA-carrying chromosome arm; **Supplementary Fig. 5** online). Although this model would imply a very high compaction (~ 0.8 kb nm^{-1}), one explanation for this linearity is that, at these scales, chromosome arms behave as rigid rods between the centromere and points up to 500 kb away from it. More experiments are required to test this hypothesis, but this example highlights the method's potential for analyzing chromosome configuration *in vivo*.

DISCUSSION

Although earlier time-lapse experiments indicated that chromatin motions are constrained over time scales of a few minutes^{25,28}, it was unclear whether confinement persists over longer time scales and whether the confining regions can occupy arbitrary subnuclear locations in different cells, allowing extensive intergenic interactions. Our maps clearly revealed small probabilistic gene territories tied to the nuclear architecture. Most territories were 2–3 times smaller than expected for a random nuclear distribution (**Table 1**). This strong compartmentalization in the small yeast nucleus places important constraints on possible interactions of genes with each other, the nucleolus or the nuclear envelope. The role of the nuclear architecture in regulating genomic information may thus be even more important than presently assumed.

We found that Pol II-transcribed genes required for ribosome biogenesis may display frequent (*HMO1*, *SNR17A-RPL33B*, *RPS5*) or rare (*RPS20*) juxtapositioning with the nucleolus, and that genomic distance to the centromere partly predicts proximity to the nucleolus. Just as the nuclear envelope is involved in positional

regulation of subtelomeric repeats and *GAL1* (refs. 11,29), we speculate that the nucleolus could act as a similar regulatory compartment for ribosomal components or processing factors whose genes are located at sufficiently large genomic distances from the centromere.

Nuclear organization in organisms such as the fission yeast *Schizosaccharomyces pombe* and *Plasmodium falciparum* might be investigated with the same mapping technique^{30,31}. The methodology could also be adapted to rod-shaped bacteria using their cylindrical geometry. Extensions to the more complex nuclei of higher eukaryotes may require localization of other nuclear bodies and would yield multidimensional distributions, which could be visualized using dimensionality-reduction techniques. Future improvements in data analysis and throughput should further increase resolution and enable analyses of subpopulations or cell-cycle dependence, as well as allow extension of the methodology to examining locus dynamics. Such developments will likely reveal even higher degrees of nuclear organization with additional functional implications.

METHODS

Software. All algorithms were developed in Matlab (MathWorks) and will be made available free of charge for academic and nonprofit use (<http://www.nucloc.org/>). Additional descriptions of the algorithms are available in **Supplementary Notes 3–6**.

Note: Supplementary information is available on the Nature Methods website.

ACKNOWLEDGMENTS

We thank M. Lelek, G. Hubert and A. Couesnon for performing imaging experiments and C. Machu, P. Roux and S. Shorte of the Plateforme d'Imagerie Dynamique (Institut Pasteur) for assistance with microscopy; R. Tilte for programming the nucleus-detection module; R. Tsien (University of California, San Diego) and F. Feuerbach (Institut Pasteur) for providing plasmids; and F. Feuerbach, K. Bystrycky, P. Thérizols, B. Zhang, D. Baddeley, A. Lesne, A. Rosa, M. Mhlanga, S. Bachelier, S. Bottani, O. Bischof and X. Darzacq for helpful suggestions or critical reading of an earlier version of the manuscript. A.B.B. was supported by fellowships from the French Ministry of Research and Technology and the German Academic Exchange Service. G.G.C. was recipient of a fellowship from the Association pour la Recherche sur le Cancer. E.F. benefited from Association pour la Recherche sur le Cancer grant 3266. T.D. was funded by Institut Pasteur. O.G. was funded by grants from Centre National de la Recherche Scientifique, Fondation pour la Recherche Médicale and Agence Nationale pour la Recherche. This work was funded by Institut Pasteur through 'Programme Transversal de Recherches' grants to O.G. and C.Z.

AUTHOR CONTRIBUTIONS

O.G. and C.Z. designed the method; C.Z. designed computational tools; A.B.B. and O.G. validated computational tools; A.B.B., G.G.C., O.G. and C.Z. designed experiments; A.B.B., G.G.C. and O.G. performed experiments; A.B.B., G.G.C., E.F. and O.G. constructed genetic tools and strains; A.B.B., G.G.C., E.F., H.B., O.G. and C.Z. analyzed and interpreted data; T.D. designed statistical tests; U.N. and J.-C.O.-M. provided initial motivation and scientific environment for research; C.Z. wrote the paper; and A.B.B., G.G.C., E.F., H.B. and O.G. edited the paper.

Published online at <http://www.nature.com/naturemethods/>
Reprints and permissions information is available online at
<http://npg.nature.com/reprintsandpermissions/>

1. Misteli, T. Beyond the sequence: cellular organization of genome function. *Cell* **128**, 787–800 (2007).
2. Lanctot, C. *et al.* Dynamic genome architecture in the nuclear space: regulation of gene expression in three dimensions. *Nat. Rev. Genet.* **8**, 104–115 (2007).
3. Fraser, P. & Bickmore, W. Nuclear organization of the genome and the potential for gene regulation. *Nature* **447**, 413–417 (2007).
4. Jhunjhunwala, S. *et al.* The 3D structure of the immunoglobulin heavy-chain locus: implications for long-range genomic interactions. *Cell* **133**, 265–279 (2008).

5. Rauch, J. *et al.* Light optical precision measurements of the active and inactive Prader-Willi syndrome imprinted regions in human cell nuclei. *Differentiation* **76**, 66–82 (2008).
6. Haber, J.E. & Leung, W.Y. Lack of chromosome territoriality in yeast: promiscuous rejoining of broken chromosome ends. *Proc. Natl. Acad. Sci. USA* **93**, 13949–13954 (1996).
7. Lorenz, A. *et al.* Spatial organisation and behaviour of the parental chromosome sets in the nuclei of *Saccharomyces cerevisiae* × *S. paradoxus* hybrids. *J. Cell Sci.* **115**, 3829–3835 (2002).
8. Robinett, C.C. *et al.* *In vivo* localization of DNA sequences and visualization of large-scale chromatin organization using lac operator/repressor recognition. *J. Cell Biol.* **135**, 1685–1700 (1996).
9. Brickner, J.H. & Walter, P. Gene recruitment of the activated INO1 locus to the nuclear membrane. *PLoS Biol.* **2**, e342 (2004).
10. Diepkins, G., Iglesias, N. & Stutz, F. Cotranscriptional recruitment to the mRNA export receptor Mex67p contributes to nuclear pore anchoring of activated genes. *Mol. Cell Biol.* **26**, 7858–7870 (2006).
11. Cabal, G.G. *et al.* SAGA interacting factors confine sub-diffusion of transcribed genes to the nuclear envelope. *Nature* **441**, 770–773 (2006).
12. Casolari, J.M. *et al.* Genome-wide localization of the nuclear transport machinery couples transcriptional status and nuclear organization. *Cell* **117**, 427–439 (2004).
13. Schmid, M. *et al.* Nup-PI: the nucleopore-promoter interaction of genes in yeast. *Mol. Cell* **21**, 379–391 (2006).
14. Taddei, A. Active genes at the nuclear pore complex. *Curr. Opin. Cell Biol.* **19**, 305–310 (2007).
15. Shiels, C. *et al.* Quantitative analysis of cell nucleus organisation. *PLoS Comput. Biol.* **3**, e138 (2007).
16. Jin, Q.W., Fuchs, J. & Loidl, J. Centromere clustering is a major determinant of yeast interphase nuclear organization. *J. Cell Sci.* **113**, 1903–1912 (2000).
17. Gotta, M. *et al.* The clustering of telomeres and colocalization with Rap1, Sir3, and Sir4 proteins in wild-type *Saccharomyces cerevisiae*. *J. Cell Biol.* **134**, 1349–1363 (1996).
18. Bystricky, K. *et al.* Chromosome looping in yeast: telomere pairing and coordinated movement reflect anchoring efficiency and territorial organization. *J. Cell Biol.* **168**, 375–387 (2005).
19. Thompson, M., Haeusler, R.A., Good, P.D. & Engelke, D.R. Nucleolar clustering of dispersed tRNA genes. *Science* **302**, 1399–1401 (2003).
20. Jorgensen, P. *et al.* A dynamic transcriptional network communicates growth potential to ribosome synthesis and critical cell size. *Genes Dev.* **18**, 2491–2505 (2004).
21. Shaner, N.C. *et al.* Improved monomeric red, orange and yellow fluorescent proteins derived from *Discosoma* sp. red fluorescent protein. *Nat. Biotechnol.* **22**, 1567–1572 (2004).
22. Yang, C.H. *et al.* Higher order structure is present in the yeast nucleus: autoantibody probes demonstrate that the nucleolus lies opposite the spindle pole body. *Chromosoma* **98**, 123–128 (1989).
23. Léger-Silvestre, I., Trumtel, S., Noaillac-Depeyre, J. & Gas, N. Functional compartmentalization of the nucleus in the budding yeast *Saccharomyces cerevisiae*. *Chromosoma* **108**, 103–113 (1999).
24. Dorn, J.F. *et al.* Yeast kinetochore microtubule dynamics analyzed by high-resolution three-dimensional microscopy. *Biophys. J.* **89**, 2835–2854 (2005).
25. Heun, P. *et al.* Chromosome dynamics in the yeast interphase nucleus. *Science* **294**, 2181–2186 (2001).
26. Osborne, C.S. *et al.* Active genes dynamically colocalize to shared sites of ongoing transcription. *Nat. Genet.* **36**, 1065–1071 (2004).
27. Berger, A.B. *et al.* Hmo1 is required for TOR-dependent regulation of ribosomal protein gene transcription. *Mol. Cell Biol.* **27**, 8015–8026 (2007).
28. Marshall, W.F. *et al.* Interphase chromosomes undergo constrained diffusional motion in living cells. *Curr. Biol.* **7**, 930–939 (1997).
29. Therizols, P. *et al.* Telomere tethering at the nuclear periphery is essential for efficient DNA double strand break repair in subtelomeric region. *J. Cell Biol.* **172**, 189–199 (2006).
30. Léger-Silvestre, I., Noaillac-Depeyre, J., Faubladier, M. & Gas, N. Structural and functional analysis of the nucleolus of the fission yeast *Schizosaccharomyces pombe*. *Eur. J. Cell Biol.* **72**, 13–23 (1997).
31. Ralph, S.A., Scheidig-Benatar, C. & Scherf, A. Antigenic variation in *Plasmodium falciparum* is associated with movement of *var* loci between subnuclear locations. *Proc. Natl. Acad. Sci. USA* **102**, 5414–5419 (2005).